



Calculation of predictions for non-identical particle correlations in AA collisions at LHC energies from hydrodynamics-inspired models

MASTER OF SCIENCE THESIS

Author:

Mateusz Wojciech Gałążyn

Supervisor:

Prof. Adam Kisiel

Warsaw, 22nd August 2014



Obliczenia teoretycznych przewidywań korelacji cząstek nieidentycznych w zderzeniach AA przy energiach LHC pochodzących z modeli hydrodynamicznych

PRACA MAGISTERSKA

Autor:

Mateusz Wojciech Gałążyn

Promotor:

dr hab. inż. Adam Kisiel, prof. PW

Warszawa, 22 sierpnia 2014

Abstract

Streszczenie

Contents

4	1 Theory of heavy ion collisions	2
5	1.1 The Standard Model	2
6	1.2 Quantum Chromodynamics	3
7	1.2.1 Quarks and gluons	3
8	1.2.2 Quantum Chromodynamics potential	4
9	1.2.3 The quark-gluon plasma	6
10	1.3 Relativistic heavy ion collisions	7
11	1.3.1 Stages of heavy ion collision	7
12	1.3.2 QGP signatures	9
13	2 Therminator model	17
14	2.1 (3+1)-dimensional viscous hydrodynamics	17
15	2.2 Statistical hadronization	18
16	2.2.1 Cooper-Frye formalism	19
17	3 Particle interferometry	21
18	3.1 HBT interferometry	21
19	3.2 Intensity interferometry in heavy ion collisions	21
20	3.2.1 Theoretical approach	21
21	3.2.2 Experimental approach	21
22	3.3 Scaling of femtoscopic radii	21
23	4 Results	22
24	4.1 Identical particles correlations	22
25	4.2 Results of the fit	22
26	4.3 Discussion of results	22
27	5 Summary	23

28 Introduction

Chapter 1

Theory of heavy ion collisions

1.1 The Standard Model

In the 1970s, a new theory of fundamental particles and their interaction emerged. A new concept, which concerns the electromagnetic, weak and strong nuclear interactions between know particles. This theory is called *The Standard Model*. There are seventeen named particles in the standard model, organized into the chart shown below (Fig. 1.1). Fundamental particles are divided into two families: *fermions* and *bosons*.



Figure 1.1: The Standard Model of elementary particles [1].

Fermions are the building blocks of matter. They are divided into two groups. Six of them, which must bind together are called *quarks*. Quarks are known to bind into doublets (*mesons*), triplets (*baryons*) and recently confirmed four-quark states.¹ Two of baryons, with the longest lifetimes, are forming a nucleus: a proton and a neutron. A proton is build from two up quarks and one down, and neutron consists of two down quarks and one up. A proton is found to be a stable particle (at least it has a lifetime larger than 10^{35} years) and a free neutron has a mean lifetime about 8.8×10^2 s. Fermions, that can exist independently are called *leptons*. Neutrinos are a subgroup of leptons, which are only influenced by weak interaction. Fermions can be divided into three generations (three columns in the Figure 1.1). Generation I particles can combine into hadrons with the longest life spans. Generation II and III consists of unstable particles which form also unstable hadrons.

Bosons are force carriers. There are four fundamental forces: weak - responsible for radioactive decay, strong - coupling quarks into hadrons, electromagnetic - between charged particles and gravity - the weakest, which causes the attraction between particles with a mass. The Standard Model describes the first three. The weak force is mediated by W^\pm and Z^0 bosons, electromagnetic force is carried by photons γ and the carriers of a strong interaction are gluons g . The fifth boson is a Higgs boson which is responsible for giving other particles mass.

1.2 Quantum Chromodynamics

1.2.1 Quarks and gluons

Quarks interact with each other through the strong interaction. The mediator of this force is a *gluon* - a massless and chargeless particle. In the quantum chromodynamics (QCD) - theory describing strong interaction - there are six types of "charges" (like electrical charges in the electrodynamics) called *colours*. The colours were introduced because some of the observed particles, like Δ^- , Δ^{++} and Ω^- appeared to consist of three quarks with the same flavour (*ddd*, *uuu* and *sss* respectively), which was in conflict with the Pauli principle. One quark can carry one of the three colours (usually called *red*, *green* and *blue*) and antiquark one of the three anti-colours respectively. Only colour-neutral (or white) particles could exist. Mesons are assumed to be a colour-anticolour pair, while baryons are *red-green-blue* triplets. Gluons also are colour-charged and there are 8 types of gluons. Therefore they can interact with themselves [3].

¹The LHCb experiment at CERN in Geneva confirmed recently existence of $Z(4430)$ - a particle consisting of four quarks [2].

1.2.2 Quantum Chromodynamics potential

As a result of that gluons are massless, one can expect, that the static potential in the QCD will have the similar form like one in the electrodynamics e.g. $\sim 1/r$ (through an analogy to photons). In reality the QCD potential is assumed to have the form of [3]

$$V_s = -\frac{4}{3} \frac{\alpha_s}{r} + kr, \quad (1.1)$$

where the α_s is a coupling constant of the strong force and the kr part is related with the *confinement*. In comparison to the electromagnetic force, a value of the strong coupling constant is $\alpha_s \approx 1$ and the electromagnetic one is $\alpha = 1/137$.

The fact that quarks does not exist separately, but they are always bound, is called a confinement. As two quarks are pulled apart, the linear part kr in the (1.1) becomes dominant and the potential becomes proportional to the distance. This situation resembles stretching of a string. At some point, when the string is so large it is energetically favourable to create a quark-antiquark pair. At this moment such pair (or pairs) is formed, the string breaks and the confinement is preserved (Fig. 1.2).

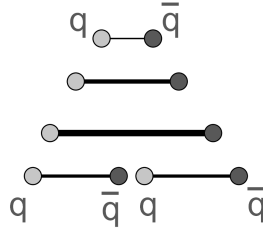


Figure 1.2: A string break and a creation of a pair quark-anti-quark [4].

On the other hand, for the small r , an interaction between the quarks and gluons is dominated by the Coulomb-like term $-\frac{4}{3} \frac{\alpha_s}{r}$. The coupling constant α_s depends on the four-momentum Q^2 transferred in the interaction. This dependence is presented in Fig. 1.3. The value α_s decreases with increasing momentum transfer and the interaction becomes weak for large Q^2 , i.e. $\alpha_s(Q) \rightarrow 0$. Because of weakening of coupling constant, quarks at large energies (or small distances) are starting to behave like free particles. This phenomenon is known as an *asymptotic freedom*. The QCD potential has also temperature dependence - the force strength “melts” with the temperature increase. Therefore the asymptotic freedom is expected to appear in either the case of high baryon densities (small distances between quarks) or very high temperatures. This temperature dependence is illustrated in the Fig. 1.4.

If the coupling constant α_s is small, one can use perturbative methods to calculate physical observables. Perturbative QCD (pQCD) successfully describes hard processes (with large Q^2), such as jet production in high energy proton-antiproton collisions. The applicability of pQCD is defined by the *scale parameter*



Figure 1.3: The coupling parameter α_s dependence on four-momentum transfer Q^2 [5].

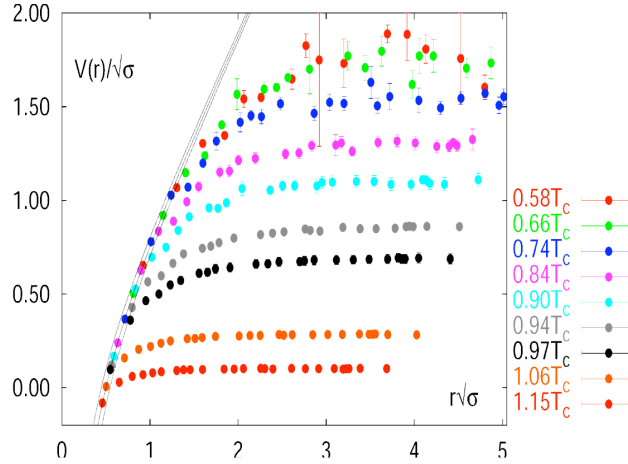


Figure 1.4: The QCD potential for a pair quark-antiquark as a function of distance for different temperatures. A value of a potential decreases with the temperature [4].

102 $\Lambda_{QCD} \approx 200$ MeV. If $Q \gg \Lambda_{QCD}$ then the process is in the perturbative domain
 103 and can be described by pQCD. A description of soft processes (when $Q < 1$ GeV)
 104 is a problem in QCD - perturbative theory breaks down at this scale. Therefore,
 105 to describe processes with low Q^2 , one has to use alternative methods like Lattice
 106 QCD. Lattice QCD (LQCD) is non-perturbative implementation of a field theory
 107 in which QCD quantities are calculated on a discrete space-time grid. LQCD al-

108 lows to obtain properties of matter in equilibrium, but there are some limitations.
 109 Lattice QCD requires fine lattice spacing to obtain precise results - therefore large
 110 computational resources are necessary. With the constant growth of computing
 111 power this problem will become less important. The second problem is that lat-
 112 tice simulations are possible only for baryon density $\mu_B = 0$. At $\mu_B \neq 0$, Lattice
 113 QCD breaks down because of the sign problem [6].

114 1.2.3 The quark-gluon plasma

115 The new state of matter in which quarks are no longer confined is known as
 116 a *quark-gluon plasma* (QGP). The predictions coming from the discrete space-time
 117 Lattice QCD calculations reveal a phase transition from the hadronic matter to
 the quark-gluon plasma at the high temperatures and baryon densities. The res-

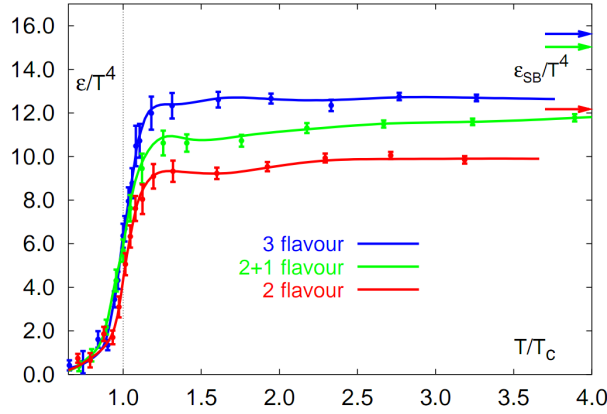


Figure 1.5: A number of degrees of freedom as a function of a temperature [7].

118 ults obtained from such calculations are shown on Fig. 1.5. The energy density
 119 ϵ which is divided by T^4 is a measure of number of degrees of freedom in the
 120 system. One can observe significant rise of this value, when the temperature in-
 121 creases past the critical value T_C . Such increase is signaling a phase transition -
 122 the formation of QGP [8]. The values of the energy densities plotted in Fig. 1.5
 123 do not reach the Stefan-Boltzmann limit ϵ_{SB} (marked with arrows), which cor-
 124 responds to an ideal gas. This can indicate some residual interactions in the system.
 125 According to the results from the RHIC², the new phase of matter behaves more
 126 like an ideal fluid, than like a gas [9].

128 One of the key questions, to which current heavy ion physics tries to find
 129 an answer is the value of a critical temperature T_C as a function of a baryon
 130 chemical potential μ_B (baryon density), where the phase transition occur. The
 131 results coming from the Lattice QCD are presented in the Fig. 1.6. The phase of
 132 matter in which quarks and gluons are deconfined is expected to exist at large

²Relativistic Heavy Ion Collider at Brookhaven National Laboratory in Upton, New York



Figure 1.6: Phase diagram coming from the Lattice QCD calculations [8].

temperatures. In the region of small temperatures and high baryon densities, a different state is supposed to appear - a *colour superconductor*. The phase transition between hadronic matter and QGP is thought to be of 1st order at $\mu_B \gg 0$. However as $\mu_B \rightarrow 0$ quarks' masses become significant and a sharp transition transforms into a rapid but smooth cross-over. It is believed that in Pb-Pb collisions observed at the LHC³, the created matter has high enough temperature to be in the quark-gluon plasma phase, then cools down and converts into hadrons, undergoing a smooth transition [8].

1.3 Relativistic heavy ion collisions

1.3.1 Stages of heavy ion collision

To create the quark-gluon plasma one has to achieve high enough temperatures and baryon densities. Such conditions can be recreated in the heavy ion collisions at the high energies. The left side of the Figure 1.7 shows simplified picture of a central collision of two highly relativistic nuclei in the centre-of-mass reference frame. The colliding nuclei are presented as thin disks because of the Lorentz contraction. In the central region, where the energy density is the highest, a new state of matter - the quark-gluon plasma - is supposedly created. Afterwards, the plasma expands and cools down, quarks combine into hadrons and their mutual interactions cease when the system reaches the *freeze-out* temperature. Subsequently, produced free hadrons move towards the detectors.

On the right side of the Figure 1.7 there is presented a space-time evolution of a collision process, plotted in the light-cone variables (z, t). The two highly

³Large Hadron Collider at CERN, Geneva

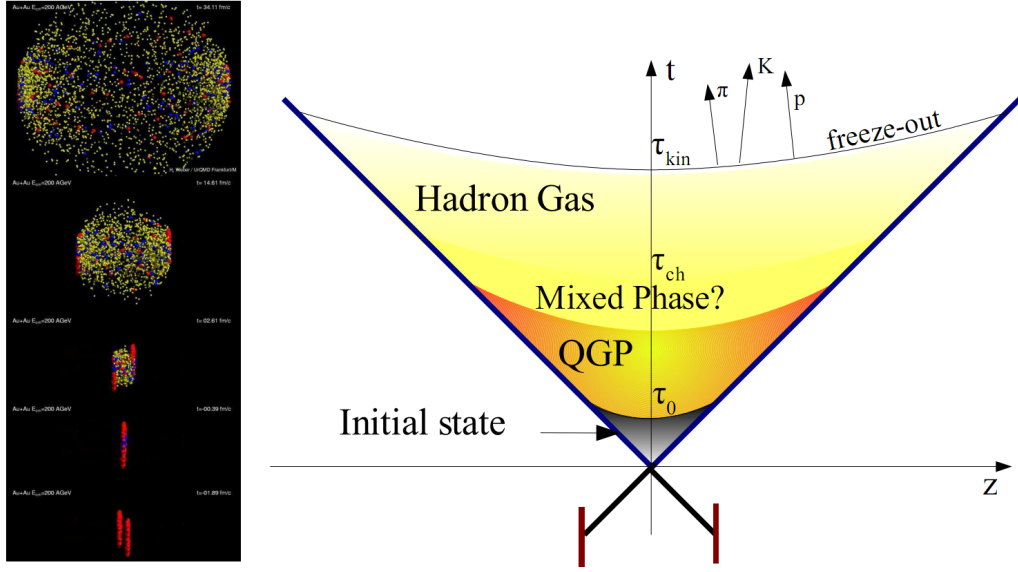


Figure 1.7: Left: stages of a heavy ion collision simulated in the UrQMD model. Right: schematic view of a heavy ion collision evolution [8].

relativistic nuclei are traveling basically along the light cone until they collide at the centre of diagram. Nuclear fragments emerge from the collision again along the (forward) light cone, while the matter between fragmentation zones populates the central region. This hot and dense matter is believed to be in the state of the quark-gluon plasma. There exist several frameworks to describe this transition to the QGP phase, for example: QCD string breaking, QCD parton cascades or colour glass condensate evolving into glasma and later into quark-gluon plasma [10].

String breaking – In the string picture, the nuclei pass through each other forming colour strings. This is analogous to the situation depicted in the Fig 1.2 - the colour string is created between quarks inside particular nucleons in nuclei. In the next step strings decay / fragment forming quarks and gluons or directly hadrons. This approach becomes invalid at very high energies, when the strings overlap and cannot be treated as independent objects.

Parton cascade – The parton⁴ cascade model is based on the pQCD. The colliding nuclei are treated as clouds of quarks and which penetrate through each other. The key element of this method is the time evolution of the parton phase-space distributions, which is governed by a relativistic Boltzmann equation with a collision term that contains dominant perturbative QCD interactions. The bottleneck of the parton cascade model is the low energies regime, where the Q^2 is too small to be described by the perturbative theory.

⁴A parton is a common name for a quark and a gluon.

176 **Colour glass condensate** – The colour glass condensate assumes, that the had-
 177 ron can be viewed as a tightly packed system of interacting gluons. The sat-
 178 uration of gluons increases with energy, hence the total number of gluons may
 179 increase without the bound. Such a saturated and weakly coupled gluon system
 180 is called a colour glass condensate. The fast gluons in the condensate are Lorentz
 181 contracted and redistributed on the two very thin sheets representing two col-
 182 liding nuclei. The sheets are perpendicular to the beam axis. The fast gluons
 183 produce mutually orthogonal colour magnetic and electric fields, that only ex-
 184 ist on the sheets. Immediately after the collision, i.e. just after the passage of
 185 the two gluonic sheets after each other, the longitudinal electric and magnetic
 186 fields are produced forming the *glasma*. The glasma fields decay through the
 187 classical rearrangement of the fields into radiation of gluons. Also decays due to
 188 the quantum pair creations are possible. In this way, the quark-gluon plasma is
 189 produced.

190 Interactions within the created quark-gluon plasma bring the system into the
 191 local statistical equilibrium, hence its further evolution can be described by the
 192 relativistic hydrodynamics. The hydrodynamic expansion causes that the sys-
 193 tem becomes more and more dilute. The phase transition from the quark-gluon
 194 plasma to the hadronic gas occurs. Further expansion causes a transition from the
 195 strongly interaction hadronic gas to weakly interacting system of hadrons which
 196 move freely to the detectors. Such decoupling of hadrons is called the *freeze-out*.
 197 The freeze-out can be divided into two phases: the chemical freeze-out and the
 198 thermal one. The *chemical freeze-out* occurs when the inelastic collisions between
 199 constituents of the hadron gas stop. As the system evolves from the chemical
 200 freeze-out to the thermal freeze-out the dominant processes are elastic collisions
 201 (such as, for example $\pi + \pi \rightarrow \rho \rightarrow \pi + \pi$) and strong decays of heavier reson-
 202 ances which populate the yield of stable hadrons. The *thermal freeze-out* is the
 203 stage of the evolution of matter, when the strongly coupled system transforms
 204 to a weakly coupled one (consisting of essentially free particles). In other words
 205 this is the moment, where the hadrons practically stop to interact. Obviously, the
 206 temperatures corresponding to the two freeze-outs satisfy the condition

$$T_{chem} > T_{therm} , \quad (1.2)$$

207 where T_{chem} (inferred from the ratios of hadron multiplicities) is the temperature
 208 of the chemical freeze-out, and T_{therm} (obtained from the investigation of the
 209 transverse-momentum spectra) is the temperature of the thermal freeze-out [10].

210 1.3.2 QGP signatures

211 The quark-gluon plasma is a very short living and unstable state of matter.
 212 One cannot investigate the properties of a plasma and confirm its existence di-
 213 rectly. Hence, the several experimental effects were proposed as QGP signatures,
 214 some of them have been already observed in heavy ion experiments [8]. As mat-
 215 ter created in the heavy ions collisions is supposed to behave like a fluid, one

216 should expect appearance of collective behaviour at small transverse momenta
 217 - so called *elliptic flow* and *radial flow*. The next signal is the temperature range
 218 obtained from the measurements of *direct photons*, which gives us information,
 219 that the system created in heavy ion collisions is far above the critical temperat-
 220 ure obtained from the LQCD calculations. The *puzzle in the di-lepton spectrum* can
 221 be explained by the modification of spectral shape of vector mesons (mostly ρ
 222 meson) in the presence of a dense medium. This presence of a medium can also
 223 shed light on the *jet quenching* phenomenon - the suppression occurrence in the
 224 high p_T domain.

225 Elliptic flow

226 In a non-central heavy ion collisions, created region of matter has an almond
 227 shape with its shorter axis in the *reaction plane* (Fig. 1.8). The pressure gradient
 228 is much larger in-plane rather than out-of-plane. This causes larger acceleration
 and transverse velocities in-plane rather than out-of-plane. Such differences can

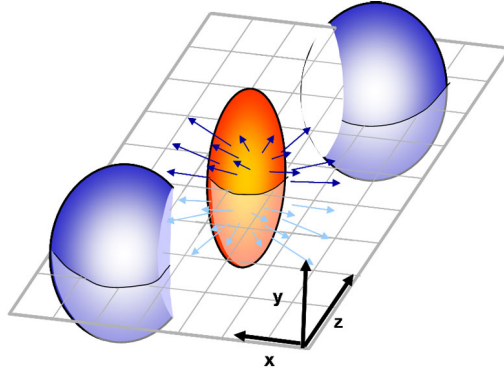


Figure 1.8: Overlapping region which is created in heavy ion collisions has an almond shape. Visible x-z plane is a *reaction plane*. The x-y plane is a *transverse plane*. The z is a direction of the beam [11].

229 be investigated by studying the distribution of particles with respect to the reac-
 230 tion plane orientation [12]:
 231

$$E \frac{d^3 N}{dp^3} = \frac{1}{2\pi} \frac{d^2 N}{p_T dp_T dy} (1 + 2v_1 \cos(\phi) + 2v_2 \cos(2\phi) + \dots), \quad (1.3)$$

232 where ϕ is the angle between particle transverse momentum p_T (a momentum
 233 projection on a transverse plane) and the reaction plane, N is a number of
 234 particles and E is an energy of a particle. The y variable is a *rapidity* defined as:

$$y = \frac{1}{2} \ln \left(\frac{E + p_L}{E - p_L} \right), \quad (1.4)$$

where p_L is a longitudinal component of a momentum (parallel to the beam direction). The v_n coefficients indicate the shape of a system. For the most central collisions ($b = 0$ - see Fig. 1.9) all coefficients vanish $\bigwedge_{n \in N_+} v_n = 0$ (the overlapping region has the spherical shape). The Fourier series elements in the parentheses

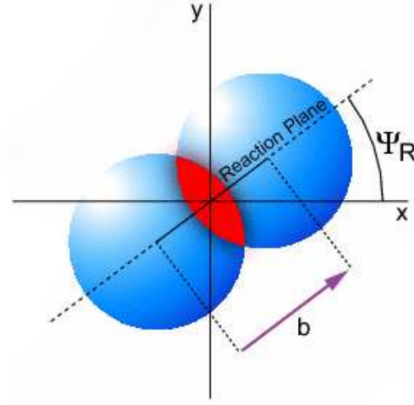


Figure 1.9: Cross-section of a heavy ion collision in a transverse plane. Ψ_R is an angle between transverse plane and the reaction plane. The b parameter is an *impact parameter* - a distance between centers of nuclei during a collision. An impact parameter is related with the centrality of a collision and a volume of the quark-gluon plasma [12].

in (1.3) represent different kinds of a flow. The first value: “1” represents the *radial flow* - an isotropic flow in every direction. Next coefficient v_1 is responsible for *direct flow*. The v_2 coefficient is a measure of elliptic anisotropy (*elliptic flow*). The v_2 has to build up in the early stage of a collision - later the system becomes too dilute: space asymmetry and the pressure gradient vanish. Therefore the observation of elliptic flow means that the created matter was in fact a strongly interacting matter.

The v_2 coefficient was measured already at CERN SPS, LHC and RHIC. For the first time hydrodynamics successfully described the collision dynamics as the measured v_2 reached hydrodynamic limit (Fig. 1.10). As expected, there is a mass ordering of v_2 as a function of p_T (lower plot in the Fig. 1.10) with pions having the largest and protons the smallest anisotropy. In the upper plots in the Fig. 1.10 there is a v_2 as a function of transverse kinetic energy. The left plot shows the two universal trend lines for baryons and mesons. After the scaling of v_2 and the kinetic energy by the number of valence quarks, all of the hadrons follow the same universal curve. Those plots show that strong collectivity is observed in heavy ion collisions.



Figure 1.10: *Lower:* The elliptic flow v_2 follows the hydrodynamical predictions for an ideal fluid perfectly. Note that $> 99\%$ of all final hadrons have $p_T < 1.5$ GeV/c. *Upper left:* The v_2 plotted versus transverse kinetic energy $KE_T = m_T - m_0 = \sqrt{p_T^2 + m_0^2} - m_0$. The v_2 follows different universal curves for mesons and baryons. *Upper right:* When scaled by the number of valence quarks, the v_2 follows the same universal curve for all hadrons and for all values of scaled transverse kinetic energy [13].

256 Transverse radial flow

257 Elliptic flow described previously is caused by the pressure gradients which
 258 must also produce a more simple collective behaviour of matter - a movement
 259 inside-out, called radial flow. Particles are pushed to higher momenta and they
 260 move away from the center of the collision. A source not showing collective

behaviour, like pp collisions, produces particle spectra that can be fitted by a power-law [8]:

$$\frac{1}{2\pi p_T} \frac{d^2 N}{dp_T d\eta} = C \left(1 + \frac{p_T}{p_0} \right)^{-n} . \quad (1.5)$$

The η variable is a *pseudorapidity* defined as follows:

$$\eta = \frac{1}{2} \ln \left(\frac{p + p_L}{p - p_L} \right) = -\ln \left(\frac{\theta}{2} \right) , \quad (1.6)$$

where θ is an emission angle $\cos \theta = p_L/p$.

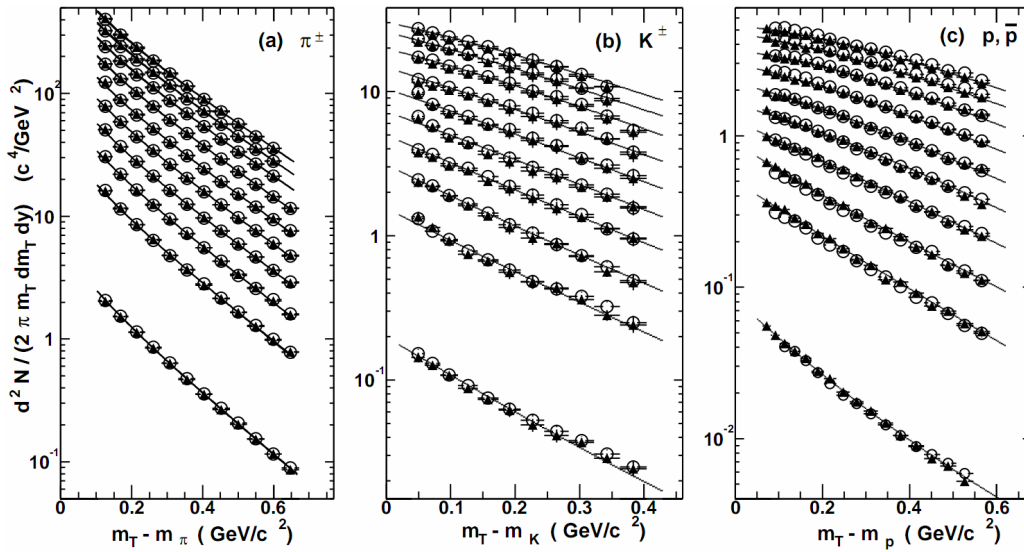


Figure 1.11: Invariant yield of particles versus transverse mass $m_T = \sqrt{p_T^2 + m_0^2}$ for π^\pm , K^\pm , p and \bar{p} at mid-rapidity for p+p collisions (bottom) and Au+Au events from 70-80% (second bottom) to 0-5% (top) centrality [14].

The hydrodynamical expansion of a system gives the same flow velocity kick for different kind of particles - ones with bigger masses will gain larger p_T boost. This causes increase of the yield of particles with larger transverse momenta. In the invariant yield plots one can observe the decrease of the slope parameter, especially for the heavier hadrons. This is presented in the Fig. 1.11. The most affected spectra are ones of kaons (b) and protons (c). One can notice decrease of the slope parameter for heavy ion collisions (plots from second bottom to top) comparing to the proton-proton collisions (bottom ones), where no boost from radial flow should occur [8].

Direct photons

The direct photons are photons, which are not coming from the final state hadrons decays. Their sources can be various interaction from charged particles

created in the collision, either at the partonic or at the hadronic level. Direct photons are considered to be an excellent probe of the early stage of the collision. This is because their mean free path is very large to the created system in the collision. Thus photons created at the early stage leave the system without suffering any interaction and retain information about this stage, in particular about its temperature.

One can distinguish two kinds of direct photons: *thermal* and *prompt*. Thermal photons can be emitted from the strong processes in the quark-gluon plasma involving quarks and gluons or hot hadronic matter (e.g. processes: $\pi\pi \rightarrow \rho\gamma$, $\pi\rho \rightarrow \pi\gamma$). Thermal photons can be observed in the low p_T region. Prompt photons are believed to come from “hard” collisions of initial state partons belonging to the colliding nuclei. The prompt photons can be described using the pQCD. They will dominate the high p_T region. The analysis of transverse momentum of spectra of direct photons revealed, that the temperature of the source of thermal photons produced in heavy ion collisions at RHIC is in the range 300–600 MeV (Fig. 1.12). Hence the direct photons had to come from a system whose temperature is far above from the critical temperature for QGP creation.

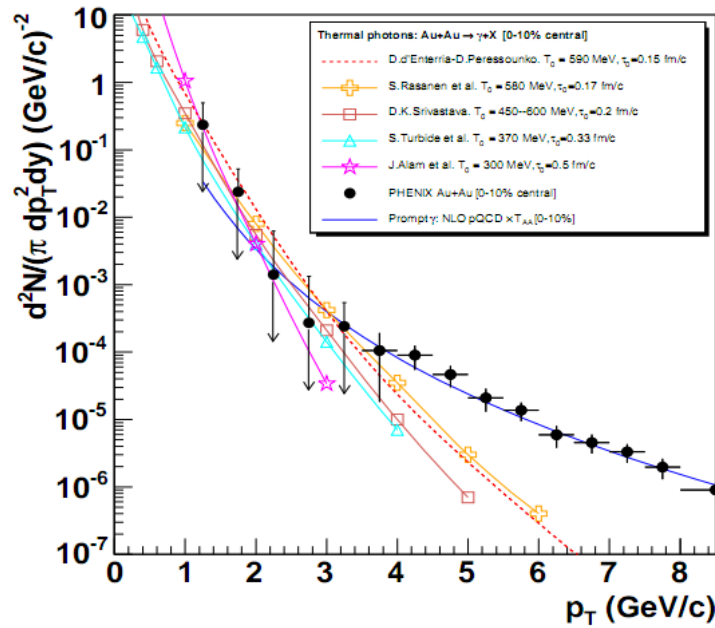


Figure 1.12: Thermal photons spectra for the central Au+Au collisions at $\sqrt{s_{NN}} = 200$ GeV at computed within different hydrodynamical models compared with the pQCD calculations (solid line) and experimental data from PHENIX (black dots) [15].

Puzzle in di-lepton mass spectrum

The invariant mass spectra (Fig. 1.13) of lepton pairs reveal many peaks corresponding to direct decays of various mesons into a lepton pair. The continuous background in this plot is caused by the decays of hadrons into more than two leptons (including so-called *Dalitz decays* into a lepton pair and a photon). Particular hadron decay channels, which contribute to this spectrum are shown

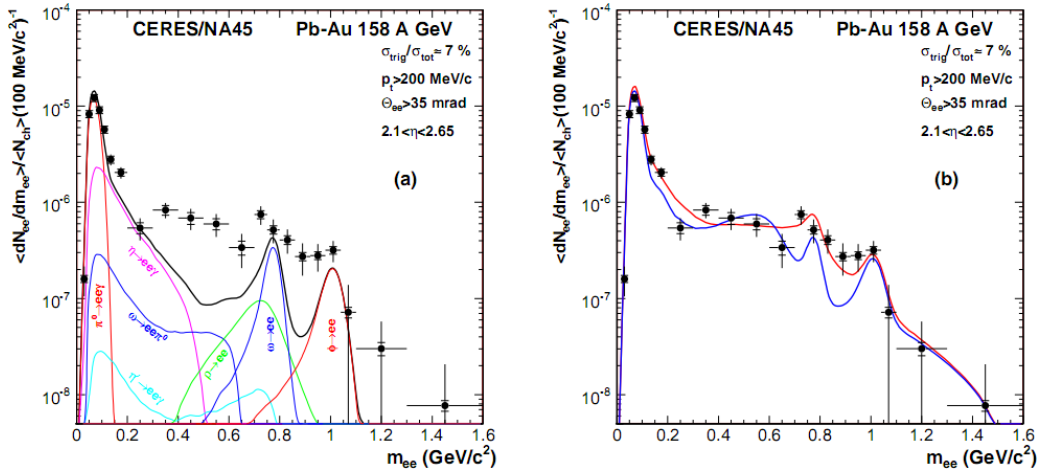


Figure 1.13: Left: Invariant mass spectrum of e^+e^- pairs in Pb+Au collisions at 158A GeV compared to the sum coming from the hadron decays predictions. Right: The expectations coming from model calculations assuming a dropping of the ρ mass (blue) or a spread of the ρ width in the medium (red) [16].

in the Fig. 1.13 with the coloured lines and their sum with the black one. The sum (called *the hadronic cocktail*) of various components describes experimental spectra coming from the simple collisions (like p+p or p+A) quite well with the statistical and systematical uncertainties [9]. This situation is different considering more complicated systems i.e. A+A. Spectra coming from Pb+Au collisions are presented on the plots in the Fig. 1.13. The “hadronic cocktail” does not describe the data, in the mass range between the π and the ρ mesons a significant excess of electron pairs over the calculated sum is observed. Theoretical explanation of this phenomenon assumes modification of the spectral shape of vector mesons in a dense medium. Two different interpretations of this increase were proposed: a decrease of meson mass with the medium density and increase of the meson width in the dense medium. In principle, one could think of simultaneous occurrence of both effects: mass shift and resonance broadening. Experimental results coming from the CERES disfavour the mass shift hypothesis indicating only broadening of resonance peaks (Fig. 1.13b) [9].

315 Jet quenching

316 A jet is defined as a group of particles with close vector momenta and high
 317 energies. It has its beginning when the two partons are going in opposite dir-
 318 ections and have energy big enough to produce new quark-antiquark pair and
 319 then radiate gluons. This process can be repeated many times and it results in
 320 two back-to-back jets of hadrons. It has been found that jets in the opposite
 321 hemisphere (*away-side jets*) show a very different pattern in d+Au and Au+Au
 322 collisions. This is shown in the azimuthal correlations in the Fig. 1.14. In d+Au
 323 collisions, like in p+p, a pronounced away-side jet appears around $\Delta\phi = \pi$, ex-
 324 actly opposite to the trigger jet, what is typical for di-jet events. In central Au+Au
 collisions the away jet is suppressed. When the jet has its beginning near the sur-

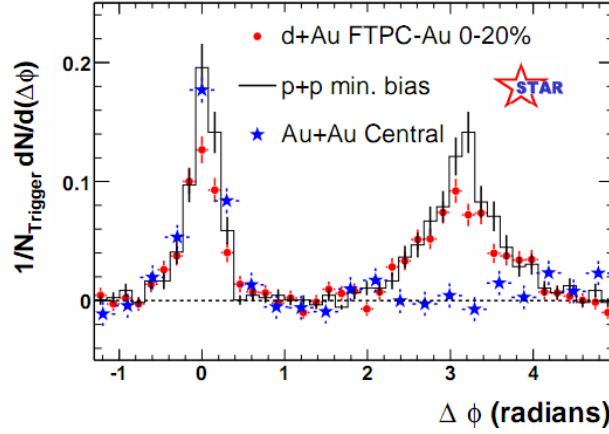


Figure 1.14: Azimuthal angle difference $\Delta\phi$ distributions for different colliding systems at $\sqrt{s_{NN}} = 200$ GeV. Transverse momentum cut: $p_T > 2$ GeV. For the Au+Au collisions the away-side jet is missing [17].

325 face of the quark-gluon plasma, one of the jets (*near-side jet*) leaves the system
 326 almost without any interactions. This jet is visible on the correlation plot as a
 327 high peak at $\Delta\phi = 0$. However, the jet moving towards the opposite direction
 328 has to penetrate a dense medium. The interaction with the plasma causes en-
 329 ergy energy losses of particles and is visible on an azimuthal correlation plot as
 330 disappearance of the away-side jet [9].

Chapter 2

Therminator model

THERMINATOR [18] is a Monte Carlo event generator designed to investigate the particle production in the relativistic heavy ion collisions. The functionality of the code includes a generation of the stable particles and unstable resonances at the chosen hypersurface model. It performs the statistical hadronization which is followed by space-time evolution of particles and the decay of resonances. The key element of this method is an inclusion of a complete list of hadronic resonances, which contribute very significantly to the observables. The second version of THERMINATOR [19] comes with a possibility to incorporate any shape of freeze-out hypersurface and the expansion velocity field, especially those generated externally with various hydrodynamic codes.

2.1 (3+1)-dimensional viscous hydrodynamics

Most of the relativistic viscous hydrodynamic calculations are done in (2+1)-dimensions. Such simplification assumes boost-invariance of a matter created in a collision. Experimental data reveals that no boost-invariant region is formed in the collisions [20]. Hence, for the better description of created system a (3+1)-dimensional model is required.

In the four dimensional relativistic dynamics one can describe a system using a space-time four-vector $x^\nu = (ct, x, y, z)$, a velocity four-vector $u^\nu = \gamma(c, v_x, v_y, v_z)$ and a energy-momentum tensor $T^{\mu\nu}$. The particular components of $T^{\mu\nu}$ have a following meaning:

- T^{00} - an energy density,
- $cT^{0\alpha}$ - an energy flux across a surface x^α ,
- $T^{\alpha 0}$ - an α -momentum flux across a surface x^α multiplied by c ,
- $T^{\alpha\beta}$ - components of momentum flux density tensor,

where $\gamma = (1 - v^2/c^2)^{-1/2}$ is Lorentz factor and $\alpha, \beta \in \{1, 2, 3\}$. Using u^ν one can express $T^{\mu\nu}$ as follows [21]:

$$T_0^{\mu\nu} = (e + p)u^\mu u^\nu - pg^{\mu\nu} \quad (2.1)$$

where e is an energy density, p is a pressure and $g^{\mu\nu}$ is an inverse metric tensor:

$$g^{\mu\nu} = \begin{bmatrix} 1 & 0 & 0 & 0 \\ 0 & -1 & 0 & 0 \\ 0 & 0 & -1 & 0 \\ 0 & 0 & 0 & -1 \end{bmatrix}. \quad (2.2)$$

The presented version of energy-momentum tensor (2.1) can be used to describe dynamics of a perfect fluid. To take into account influence of viscosity, one has to apply the following corrections coming from shear $\pi^{\mu\nu}$ and bulk Π viscosities [22]:

$$T^{\mu\nu} = T_0^{\mu\nu} + \pi^{\mu\nu} + \Pi(g^{\mu\nu} - u^\mu u^\nu). \quad (2.3)$$

The stress tensor $\pi^{\mu\nu}$ and the bulk viscosity Π are solutions of dynamical equations in the second order viscous hydrodynamic framework [21]. The comparison of hydrodynamics calculations with the experimental results reveal, that the shear viscosity divided by entropy η/s has to be small and close to the AdS/CFT estimate $\eta/s = 0.08$ [22, 23].

When using $T^{\mu\nu}$ to describe system evolving close to local thermodynamic equilibrium, relativistic hydrodynamic equations in a form of:

$$\partial_\mu T^{\mu\nu} = 0 \quad (2.4)$$

can be used to describe the dynamics of the local energy density, pressure and flow velocity.

Hydrodynamic calculations are starting from the Glauber¹ model initial conditions. The collective expansion of a fluid ends at the freeze-out hypersurface. That surface is usually defined as a constant temperature surface, or equivalently as a cut-off in local energy density. The freeze-out is assumed to occur at the temperature $T = 140$ MeV.

2.2 Statistical hadronization

Statistical description of heavy ion collision has been successfully used to describe quantitatively *soft* physics, i.e. the regime with the transverse momentum not exceeding 2 GeV. The basic assumption of the statistical approach of evolution of the quark-gluon plasma is that at some point of the space-time evolution of the fireball, the thermal equilibrium is reached. When

¹The Glauber Model is used to calculate “geometrical” parameters of a collision like an impact parameter, number of participating nucleons or number of binary collisions.

the system is in the thermal equilibrium the local phase-space densities of particles follow the Fermi-Dirac or Bose-Einstein statistical distributions. At the end of the plasma expansion, the freeze-out occurs. The freeze-out model incorporated in the THERMINATOR model assumes, that chemical and thermal freeze-out occur at the same time.

2.2.1 Cooper-Frye formalism

The result of the hydrodynamic calculations is the freeze-out hypersurface Σ^μ . A three-dimensional element of the surface is defined as [19]

$$d\Sigma_\mu = \epsilon_{\mu\alpha\beta\gamma} \frac{\partial x^\alpha}{\partial \alpha} \frac{\partial x^\beta}{\partial \beta} \frac{\partial x^\gamma}{\partial \gamma} d\alpha d\beta d\gamma, \quad (2.5)$$

where $\epsilon_{\mu\alpha\beta\gamma}$ is the Levi-Civita tensor and the variables $\alpha, \beta, \gamma \in \{1, 2, 3\}$ are used to parametrize the three-dimensional freeze-out hypersurface in the Minkowski four-dimensional space. The Levi-Civita tensor is equal to 1 when the indices form an even permutation (eg. ϵ_{0123}), to -1 when the permutation is odd (e.g. ϵ_{2134}) and has a value of 0 if any index is repeated. Therefore [19],

$$d\Sigma_0 = \begin{vmatrix} \frac{\partial x}{\partial \alpha} & \frac{\partial x}{\partial \beta} & \frac{\partial x}{\partial \gamma} \\ \frac{\partial y}{\partial \alpha} & \frac{\partial y}{\partial \beta} & \frac{\partial y}{\partial \gamma} \\ \frac{\partial z}{\partial \alpha} & \frac{\partial z}{\partial \beta} & \frac{\partial z}{\partial \gamma} \end{vmatrix} d\alpha d\beta d\gamma \quad (2.6)$$

and the remaining components are obtained by cyclic permutations of t, x, y and z .

One can obtain the number of hadrons produced on the hypersurface Σ^μ from the Cooper-Frye formalism. The following integral yields the total number of created particles [19]:

$$N = (2s + 1) \int \frac{d^3p}{(2\pi)^3 E_p} \int d\Sigma_\mu(x) p^\mu f(x, p), \quad (2.7)$$

where

$$f(p \cdot u) = \left\{ \exp \left[\frac{p_\mu u^\mu - (B\mu_B + I_3\mu_{I_3} + S\mu_S + C\mu_C)}{T} \right] \pm 1 \right\}^{-1} \quad (2.8)$$

is the phase-space distribution for particles (for stable ones and resonances). For the Fermi-Dirac distribution in the 2.8 there is a plus sign and for Bose-Einstein statistics minus sign respectively. The thermodynamic quantities appearing in the $f(\cdot)$ are T - temperature, μ_B - baryon chemical potential, μ_{I_3} - isospin chemical potential, μ_S - strange chemical potential, μ_C - charmed chemical potential and the s is a spin of a particle. One can simply derive from equation 2.7, the dependence of the momentum density [24]:

$$E \frac{dN}{d^3p} = \int f(x, p) p^\mu d\Sigma_\mu. \quad (2.9)$$

412 The equations presented above are directly used in the THERMINATOR to generate
413 the hadrons with the Monte-Carlo method.

Chapter 3

Particle interferometry

3.1 HBT interferometry

3.2 Intensity interferometry in heavy ion collisions

3.2.1 Theoretical approach

Two particle wave function

Source function

Theoretical correlation function

Spherical harmonics decomposition of correlation function

3.2.2 Experimental approach

3.3 Scaling of femtoscopic radii

425 **Chapter 4**

426 **Results**

427 **4.1 Identical particles correlations**

428 **4.2 Results of the fit**

429 **4.3 Discussion of results**

430 **Chapter 5**

431 **Summary**

Bibliography

- [1] Standard Model of Elementary Particles - Wikipedia, the free encyclopedia
http://en.wikipedia.org/wiki/standard_model.
- [2] R. Aaij et al. (LHCb Collaboration). Observation of the resonant character of the $z(4430)^-$ state. *Phys. Rev. Lett.*, 112:222002, Jun 2014.
- [3] Donald H. Perkins. *Introduction to High Energy Physics*. Cambridge University Press, fourth edition, 2000. Cambridge Books Online.
- [4] G. Odyniec. *Phase Diagram of Quantum Chromo-Dynamics* - course at Faculty of Physics, Warsaw University of Technology, Jun 2012.
- [5] J. Beringer et al. (Particle Data Group). The Review of Particle Physics. *Phys. Rev.*, D86:010001, 2012.
- [6] Z. Fodor and S.D. Katz. The Phase diagram of quantum chromodynamics. 2009.
- [7] F. Karsch. Lattice results on QCD thermodynamics. *Nuclear Physics A*, 698(1-4):199 – 208, 2002.
- [8] Adam Kisiel. *Studies of non-identical meson-meson correlations at low relative velocities in relativistic heavy-ion collisions registered in the STAR experiment*. PhD thesis, Warsaw University of Technology, Aug 2004.
- [9] J. Bartke. *Relativistic Heavy Ion Physics*. World Scientific Pub., 2009.
- [10] W. Florkowski. *Phenomenology of Ultra-Relativistic Heavy-Ion Collisions*. World Scientific, 2010.
- [11] Science Grid This Week, October 25, 2006 - Probing the Perfect Liquid with the STAR Grid
http://www.interactions.org/sgtw/2006/1025/star_grid_more.html.
- [12] K. Grebieszko. Fizyka zderzeń ciężkich jonów,
<http://www.if.pw.edu.pl/~kperl/hip/hip.html>.
- [13] Ulrich W. Heinz. From SPS to RHIC: Maurice and the CERN heavy-ion programme. *Phys.Scripta*, 78:028005, 2008.

- 460 [14] J. Adams et al. Identified particle distributions in pp and Au+Au collisions
461 at $s(\text{NN})^{1/2} = 200$ GeV. *Phys.Rev.Lett.*, 92:112301, 2004.
- 462 [15] G. David, R. Rapp, and Z. Xu. Electromagnetic Probes at RHIC-II. *Phys.Rept.*,
463 462:176–217, 2008.
- 464 [16] A. Marin et al. Dilepton measurements with CERES. *PoS*, CPOD07:034,
465 2007.
- 466 [17] John Adams et al. Experimental and theoretical challenges in the search for
467 the quark gluon plasma: The STAR Collaboration’s critical assessment of the
468 evidence from RHIC collisions. *Nucl.Phys.*, A757:102–183, 2005.
- 469 [18] Adam Kisiel, Tomasz Taluc, Wojciech Broniowski, and Wojciech
470 Florkowski. THERMINATOR: THERMal heavy-IoN generATOR. *Com-
471 put.Phys.Commun.*, 174:669–687, 2006.
- 472 [19] Mikolaj Chojnacki, Adam Kisiel, Wojciech Florkowski, and Wojciech Bro-
473 niowski. THERMINATOR 2: THERMal heavy IoN generATOR 2. *Com-
474 put.Phys.Commun.*, 183:746–773, 2012.
- 475 [20] I. et al (BRAHMS Collaboration) Bearden. Charged meson rapidity distri-
476 butions in central Au + Au collisions at $\sqrt{s_{\text{NN}}} = 200$ GeV. *Phys. Rev. Lett.*,
477 94:162301, Apr 2005.
- 478 [21] W. Israel and J.M. Stewart. Transient relativistic thermodynamics and kin-
479 etic theory. *Annals of Physics*, 118(2):341 – 372, 1979.
- 480 [22] Piotr Bozek. Flow and interferometry in (3 + 1)-dimensional viscous hydro-
481 dynamics. *Phys. Rev. C*, 85:034901, Mar 2012.
- 482 [23] K. Kovtun, P. D. T. Son, and A. O. Starinets. Viscosity in strongly interacting
483 quantum field theories from black hole physics. *Phys. Rev. Lett.*, 94:111601,
484 Mar 2005.
- 485 [24] Fred Cooper and Graham Frye. Single-particle distribution in the hydro-
486 dynamic and statistical thermodynamic models of multiparticle production.
487 *Phys. Rev. D*, 10:186–189, Jul 1974.

List of Figures

489	1.1	The Standard Model of elementary particles [1].	2
490	1.2	A string break and a creation of a pair quark-anti-quark [4].	4
491	1.3	The coupling parameter α_s dependence on four-momentum transfer Q^2 [5].	5
492			
493	1.4	The QCD potential for a pair quark-antiquark as a function of distance for different temperatures. A value of a potential decreases with the temperature [4].	5
494			
495			
496	1.5	A number of degrees of freedom as a function of a temperature [7].	6
497	1.6	Phase diagram coming from the Lattice QCD calculations [8]. . . .	7
498	1.7	Left: stages of a heavy ion collision simulated in the UrQMD model. Right: schematic view of a heavy ion collision evolution [8].	8
499			
500	1.8	Overlapping region which is created in heavy ion collisions has an almond shape. Visible x-z plane is a <i>reaction plane</i> . The x-y plane is a <i>transverse plane</i> . The z is a direction of the beam [11].	10
501			
502			
503	1.9	Cross-section of a heavy ion collision in a transverse plane. Ψ_R is an angle between transverse plane and the reaction plane. The b parameter is an <i>impact parameter</i> - a distance between centers of nuclei during a collision. An impact parameter is related with the centrality of a collision and a volume of the quark-gluon plasma [12].	11
504			
505			
506			
507			
508	1.10	<i>Lower:</i> The elliptic flow v_2 follows the hydrodynamical predictions for an ideal fluid perfectly. Note that $> 99\%$ of all final hadrons have $p_T < 1.5$ GeV/c. <i>Upper left:</i> The v_2 plotted versus transverse kinetic energy $KE_T = m_T - m_0 = \sqrt{p_T^2 + m_0^2} - m_0$. The v_2 follows different universal curves for mesons and baryons. <i>Upper right:</i> When scaled by the number of valence quarks, the v_2 follows the same universal curve for all hadrons and for all values of scaled transverse kinetic energy [13].	12
509			
510			
511			
512			
513			
514			
515			
516	1.11	Invariant yield of particles versus transverse mass $m_T = \sqrt{p_T^2 + m_0^2}$ for π^\pm , K^\pm , p and \bar{p} at mid-rapidity for p+p collisions (bottom) and Au+Au events from 70-80% (second bottom) to 0-5% (top) centrality [14].	13
517			
518			
519			

520	1.12 Thermal photons spectra for the central Au+Au collisions at	
521	$\sqrt{s_{NN}} = 200$ GeV at computed within different hydrodynamical	
522	models compared with the pQCD calculations (solid line) and	
523	experimental data from PHENIX (black dots) [15].	14
524	1.13 Left: Invariant mass spectrum of e^+e^- pairs in Pb+Au collisions	
525	at 158A GeV compared to the sum coming from the hadron decays	
526	predictions. Right: The expectations coming from model calcula-	
527	tions assuming a dropping of the ρ mass (blue) or a spread of the	
528	ρ width in the medium (red) [16].	15
529	1.14 Azimuthal angle difference $\Delta\phi$ distributions for different colliding	
530	systems at $\sqrt{s_{NN}} = 200$ GeV. Transverse momentum cut: $p_T > 2$	
531	GeV. For the Au+Au collisions the away-side jet is missing [17]. . .	16